

Segmentation and Classification of Brain Tumor using Machine Learning and Deep Learning based Inception Model

R. Aruna Kirithika¹, S. Sathiya², M. Balasubramanian³,
P. SIVARAJ⁴

¹PhD scholar in Computer and Information Science,

²Assistant Professor in Computer Science Engineering,

³Associate Professor in Computer Science Engineering,

⁴Associate Professor in Manufacturing engineering,

^{1,2,3,4}Annamalai University, Tamil Nadu, India.

E-mail: 1ashassss79@gmail.com, 2sathiya.sep05@gmail.com,

3balu_june1@gmail.com,

4cemajorsiva@gmail.com

Abstract-- In recent times, Brain Tumor(BT) has become a common phenomenon affecting almost all age group of people. Identification of this deadly disease using computer tomography, magnetic resonance imaging are very popular now-a-days. Developing a computer aided design (CAD) tool for diagnosis and classification of BT has become vital. This paper focuses on designing a tool for diagnosis and classification of BT using deep learning (DL) models, which involves a series of steps via acquiring (CT) image, preprocessing, segmenting and classifying to identify the type of tumor using SIFT with DL based Inception network model. The proposed model uses fuzzy C means algorithm for segmenting area of interest from the BT image acquired. Techniques like Gaussian Naïve Bayes (GNB) and logistic regression (LR) are used for classification processes. To ascertain all the techniques for its efficiency a benchmark dataset was used. The simulation outcome ensured that the performance of the proposed method with maximum sensitivity of 100%, specificity of 97.41%% and accuracy of 97.96%.

Keywords: Brain Tumor, Deep Learning, Feature extraction, Fuzzy C means, Inception V3, SIFT, Gaussian Naïve Bayes, Logistic Regression.

I. INTRODUCTION

In human body, brain is a vital organ which acts as a central nervous system. It controls and directs the body to function properly. Since brain is an important organ, it has to be covered from harm and ailments. Few of the brain tumors are Meningioma, Glioma, and Pituitary. Firstly, Meningiomas are prominent diseases; however, it is a non-cancerous type of tumors developed in narrow walls around the brain tissues and cells [1]. Brain Tumors (BTs) are considered to be most dreadful disease which mitigates the lifetime of a human being within a short span of time. Earlier prediction of BT is highly essential and significant to extend the patient's lifespan. This is accomplished by using Magnetic Resonance Imaging (MRI) scanning model which is applied extensively by radiologists in order to examine the BT. Finally; the scan report shows whether the brain is healthy or unhealthy. Followed by, it also finds the class of tumors when it is affected by a disorder. Fig.1. depicts the images of normal, Benign and Malignant tumor captured from computer tomography(CT). Under the application of Machine Learning (ML), MRI reports should have a précised image for predicting BT. Initially, developer's assumed 3 portions namely, Pre-processing of MRI, Feature generation, and extraction as well as Classification.

Ultimately, Median Filter (MF) has been applied to enhance the superiority of images and to conserve the edges in pre-processing phase [2]. Then, image segmentation is performed with the help of K-Means, Fuzzy C Means (FCM), and so on offers more advantageous

features from applied images. It is one of the viable and important phase which helps in image examination and interpretation. Also, it is employed extensively in brain imaging functions like tissue classification, tumor position, evaluating the volume of tumor, blood cell inclination, surgical plans, and matching. In [3], BT segmentation was utilized by a Convolutional Neural Networks (CNN) to 3D MRI. Automated prediction of brain's anatomical structure by using Deep Neural Network (DNN) was projected in [4]. In [5], a voting scheme for ensemble of transparent structures like intensity and adaptive shape modes takes place with the integration of discrete gaussian as well as higherorder patterns like Markov-Gibbs random field classification was developed. The hybridization of deep auto-encoder in conjunction with Bayesian fuzzy clustering-relied segmentation mechanism has been established in [6].

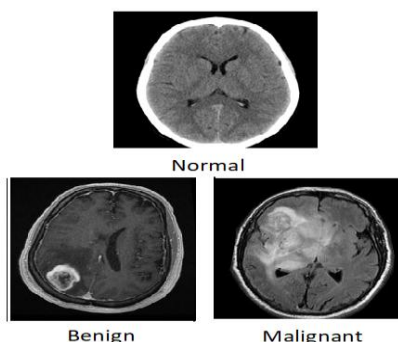


Fig.1. Images of Normal, Benign and Malignant tumor

In [7], 2D MRI is divided as left and right hemisphere along with some statistical properties was estimated for SVM classification approach. As there are massive features, feature extraction is performed with valid data under the application of Principal Component Analysis (PCA), Scale Invariant Feature Transform (SIFT), and Speed-up Robust Features (SURF) descriptors. In [8], after computing hybrid feature extraction and covariance matrix, a regularized extreme learning has been employed for classifying the brain disorder. Evolutionary Algorithms (EA) namely Particle Swarm Optimization (PSO) was utilized in [9] deciding combination of features. Moreover, well-known ML approaches are applied for image analysis.

This study introduces a novel BT diagnosis model using SURF and Inception networks. The presented model consists of preprocessing, segmentation, feature extraction, and classification. The proposed model uses FCM as a segmentation model to determine the affected tumor regions in the brain area. Besides, the SURF and Inception v3 model is employed to perform feature extraction. Finally, gaussian naïve bayes (GNB) and logistic regression (LR) classifiers are employed as classifier models to determine the distinct class labels. In order to validate the results analysis of the proposed model, a series of experiments take place on the benchmark test dataset.

II. LITERATURE REVIEW

This section performs a short survey of different ML and deep learning (DL) based BT diagnosis models available in the literature. In [10], feature extraction was applied where

brain system interface which undergoes classification using support vector machine (SVM) and Linear Discriminant Analysis (LDA). In recent times, CNN is one of the popular mechanisms with respect to feature extraction under various studies like clinical images, video examination, and natural language processing (NLP). The key objective of CNN is to forecast the chief patterns and data from training images. For example, VGGNet, GoogleNet, and AlexNet are some of the effectual structures applied in image classification which is also employed for BT prediction.

In [11], pre-processing as well as datapreparation using 3D-filters and CNN with multipath and cascadedstructures has been presented. In pixel, CNN structure was utilized for generating diverse portraits of same person with distinct poses. In [12], a pretrained CNN was employed for BT classification with DNN and SVM. Then, in [13], cascade CNNproduced a room decoration. As CNN is expensive, developers concentrated in developing cost-effective methods with exact tumor classification. The common technique is to apply ensemble of tiny collaborative learners rather than using a hectic system, in order to deal with robust training execution as well as convergence. Therefore, learning process of peer networks could be autonomous.

In [14], a KullbackLeibler divergence has been applied for matching the probability estimates of peers in supervised learning. Besides, in [15], multipath learners are involved in the outputs of shared layers. The main aim of this model is detecting the disorder robustly and maintainstumor development within a limited extent. A major challenge in ML model is to evaluate the data distribution. For instance, hardcoded associations between every image pixel and the neighbors are complicated to identify with no advanced knowledge. Additionally, autoregressive approaches are data-driven estimators used to identify these associations with typical information. Next, the produced results have enhanced images with limited noise and outlier. The density estimator tries to resolve various classifications, regression, missing data, and issues. In [16], a quantum variationalautoencoder(AE) was presented where the latent generative computation which acts as a quantum Boltzmann machine. By the estimation of BT from MRI, tiny training inputs, various shapes of tumors, and irregular information could be identified for every class. Neural Autoregressive Distribution Estimation is one of the density estimators evolved from Restricted Boltzmann machines (RBM). It is used in estimating the density of binary, real-value data, and alternate network structures like CNN. Afterward, DNN is capable of handling nonlinear conversion, sequence modeling, representation learning and it is also stretchy for learning data from real-time classification as well as recommender systems.

III. THE PROPOSED METHOD

Fig. 2 depicts the block diagram of the presented model, involving its different sub processes. Primarily, the input image is pre-processedfor stripping the skull, remove the noise, and increase the contrast level. Then, FCM based segmentation technique is employed to identify the diseased portions in the image. Afterward, the SURF and Inception v3 models are applied to extract a useful set of feature vectors. At last, GNB and LR models are utilized inclassification processes.

A. Image Pre-processing

Initially, the preprocessing of input images takes place in three different ways: skull stripping, noise removal using bilateral filtering (BF), and contrast limited adaptive histogram equalization (CLAHE) based contrast enhancement. Next to image preprocessing, segmentation task is done to identify the affected tumor regions. The segmentation process is carried out as a separate work as indicated in the [28]. A vivid explanation of the pre-processing is given earlier module.

B. Fuzzy CMeans based Segmentation

The Fuzzy CMeans (FCM) technique is applied to segment the pre-processed image. FCM is a well-known approach evolved from unsupervised ML method that is extensively used for image segmentation. Fuzzy clustering ensures to be more flexible to overcome the inaccuracy of geographical data with remote sensing data. It is significantly applied in massive data analysis, Data Mining (DM), Vector Quantization (VQ), image segmentation, and pattern detection with real-time and theoretical values.

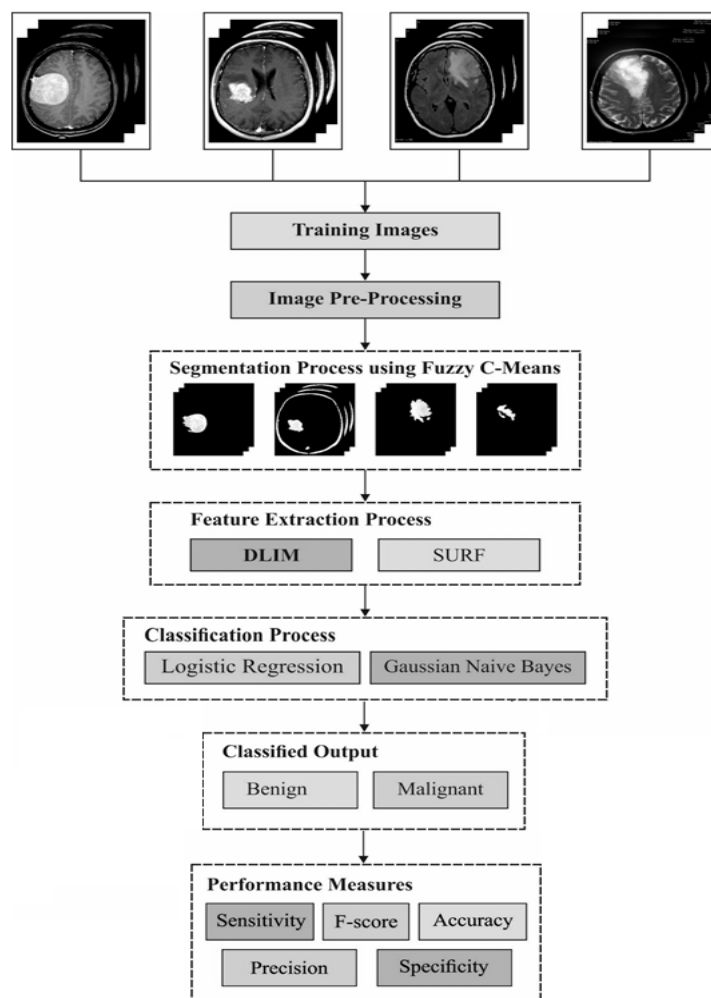


Fig. 2. Working process of presented model

According to this mechanism, fuzzy clustering contains a fuzzy set and an image pixel with a membership value related with a cluster from 0 and 1 where it measures the pixels which belong to specific cluster. Traditionally, diverse optimization models of fuzzy clustering were projected in which random projection as well as autonomous component analysis is employed for enhancing the efficiency of FCM and metaheuristic approaches are integrated with FCM to maximize the clustering performance. Fig. 3 shows the flowchart of FCM model.

Consider that $X = \{X_1, X_2, \dots, X_n\}$ implies a collection of n data points and objective function of the FCM model is expressed below:

$$J_m(U, V) = \sum_{i=1}^c \sum_{k=1}^n (u_{ik})^m d_{ik}^2(x_k, v_i), \quad (1)$$

$$d_{ik} = \|x_k - v_i\| = (x_k - v_i)^T(x_k - v_i), \quad (2)$$

where c denotes the cluster count, u_{ik} refers the membership degree of x_k in j^{th} cluster. At the same time, the measure of u_{ik} is ranged from $[0,1]$, m refers to the weighting exponent on all fuzzy memberships with a measure of 2, v_i represents j^{th} cluster center, d_{ik} exhibits the Euclidean distance among a cluster center v_i and object x_k , and $\|\cdot\|$ signifies the Euclidean norm. Furthermore, the membership function showcases the possibility of a cluster when pixels are placed away from cluster centers with limited membership values and pixels in local neighborhood of cluster centers with maximum membership value, and minimization condition has been attained [17]. In case of FCM approach, it depends upon the primary parameter set and computes the lower objective function $J_m(U, V)$ in all iterations. The U and V is described as follows:

$$u_{ik} = \begin{cases} \frac{1}{\frac{\sum_{j=1}^c (d_{jk})^2}{d_{jk}^{m-1}}}, & d_{jk} \\ 1, & d_{jk} = 0, j = k \\ 0, & d_{jk} = 0, j \neq k, \end{cases} \quad (3)$$

$$v_i = \frac{\sum_{k=1}^n (u_{ik})^m x_k}{\sum_{k=1}^n (u_{ik})^m}, \quad (4)$$

where u_{ik}, v_i implies the membership function and cluster centers, correspondingly.

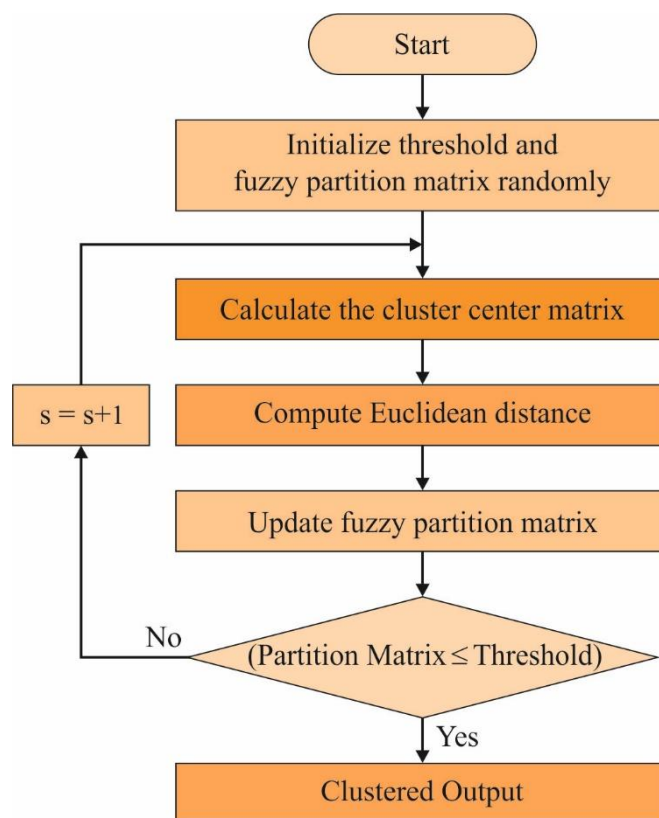


Fig. 3. Flowchart of FCM

C. Feature extraction

This section explains the two main feature extraction techniques namely SURG and Inception v3 model.

1) Speeded-Up Robust Feature model:

It is a local feature extraction technique, which makes use of a local invariant fast keypoint detection process to extract the key points of the image features. The Speeded-Up Robust Feature(SURF) is composed of 4 main phases namely, scale-space feature extraction by robust Hessian detector, extraction of keypoint, orientation schedule, as well as key point descriptor. It exploits Lowe’s suggestion named as Best-Bin-First approach, which has a distance ratio from 0.6–0.8 among closest features which is a standard matching attribute.

1. SURF feature point prediction model depends upon scale-space theory where it applies the determinant of Hessian matrix H in the form of discriminant to seek higher measures. For a point $P = \{x, y\}$ in image I , it is expressed as,

$$H(P, \sigma) = \begin{bmatrix} L_{xx}(P, \sigma)L_{xy}(P, \sigma) \\ L_{xy}(P, \sigma)L_{yy}(P, \sigma) \end{bmatrix} \quad (5)$$

Where $L_{xx}(P, \sigma)$ denotes the convolution of Gaussian 2nd order derivative with image I in point x which has been illustrated as follows

$$L_{xx}(P, \sigma) = I * \frac{\partial^2}{\partial x^2} g(\sigma) \quad (6)$$

$L_{yy}(P, \sigma)$ and $L_{xy}(P, \sigma)$ is same as $L_{xx}(P, \sigma)$. The integral image defined in [18] is used for enhancing the convolution for enhancing the processing efficiency. Furthermore, resolving and accomplishing Hessian matrix Δ function:

$$\det(H_{approx}) = D_{xx}D_{yy} - (c0D_{xy})^2 \quad (7)$$

Followed by, a spot's response measures, ω implies a value as 0.9.

2. Allocating a threshold to the Hessian matrix for the predicted extreme points. If a value is exceeds a threshold value, nonmaxima suppression has been employed for accomplishing extreme points from the neighborhood of 3D.
3. SURF descriptor depends upon the grayneighborhood statistic details inside interest points, and it is attained by measuring direction as well as feature vector. Initially, assume the feature point as a center, to measure the Harr wavelet responses in x and y direction inside a circular neighborhood with a radius $6s$ over the interest pointsimplies the scale where interest point has been predicted. Additionally, allocate Gaussian weighting coefficient for all these responses. Next, the weighted Harr wavelet response along with a histogram is employed. Followed by, collect the responses from 60° and develop a novel vector. As a result, the prolonged vector in a direction as major feature points has been utilized. U -SURF is evolved from SURF which is applied if the little rotation is absent.
4. For extracting the descriptor, initially, it is composed of making square region-based point $P(x, y)$ from a scale s , the interest points as well as selected orientation. Then, it is also intended to develop a square region of size $20 s$. Every region is classified as 4×4 square sub-regions. The sub-region is assumed as anregion with 4 elements. In all sub-regions, a Haar wavelet response has been processed at 5×5 correctly spaced instances. Hence, Haar wavelet responses for x and y elements, d_x and d_y , for sample points of responses are measured as:

$$V_{sub} = \left(\sum d_x, \sum d_y, \sum |d_x|, \sum |d_y| \right) \quad (8)$$

Results for surf feature extraction:

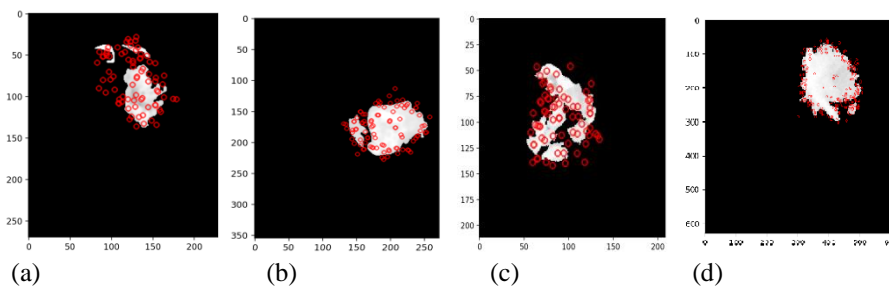


Fig.4. Feature selection from SURF (a),(b) Begnintumor (c),(d) Malignant tumor

The above fig 4. Shows the selected features from the segmented image of tumor image. The selection includes keypoints selections as indicated by the SURF feature extractor. Thus selecting the edge points in the

2) *Inception v3 model:*

CNNs developed as a multi-layer interconnected NN, where powerful low-, intermediate-, and high-level features were extracted hierarchically. A common CNN model is composed of 2 layers namely, convolutional and pooling layers which are jointly named as convolutional bases of a system [19]. Few modules like AlexNet and VGG are implanted with Fully Connected (FC) layers. First, the convolutional layer is applied to extract the spatial characteristics from the images. Typically, initial convolutional layers filter out the low-level features like edges and corners whereas the final convolutional layers filter the high-level features like image structures. It is recommended by its maximum efficiency of CNNs to learn the spatial hierarchical patterns. Also, it is operated on 2 elements namely, convolution patch size as well as and depth of last feature map which represents the filter count.

A non-linearity function like Rectified Linear Unit (ReLU) is typically employed as an element-wise nonlinear activation function for an element in the feature map.

Under the application of typical pixels, various feature maps are generated with identical function where it recommends repeated details. Thus, pooling layers are employed after convolutional layer for reducing the variance of extracted features by applying typical procedures like major averaging pooling. Initially, max- and average-pooling layers are responsible to compute both maximum and mean scores, correspondingly, with the help of fixed-size sliding window as well as classical stride across feature maps and thus it is conceptually same as convolutional layer. Unlike the convolutional layers, a stride 2 has been utilized in pooling layers for downsampling the feature map. It is evident that pooling or subsampling layer normalizes a simulation outcome of convolutional layer as higher level and decides robust as well as abstract features for upcoming layers. Hence, pooling layer reduces the processing complexity at the time of training phase by limiting the feature maps.

Followed by, few systems are comprised of FC layers in prior to classifier layer which links the final outcome of various stacked convolutional as well as pooling layers to a classifier layer. As a result, over-fitting is contributed in FC layer as it fills maximum parameters. Therefore, a dropout model is an effective regularization approach which is applicable to reduce the issues related with over-fitting. In case of training, a method which randomly drops few neurons and its connections over the system which eliminates neurons from additional co-adaptation and involves in making useful independent attributes. Consequently, classifier layer is responsible to compute the posterior probabilities to all classes. Also, softmax classifier is named as normalized exponential which is typically employed when compared with DL model.

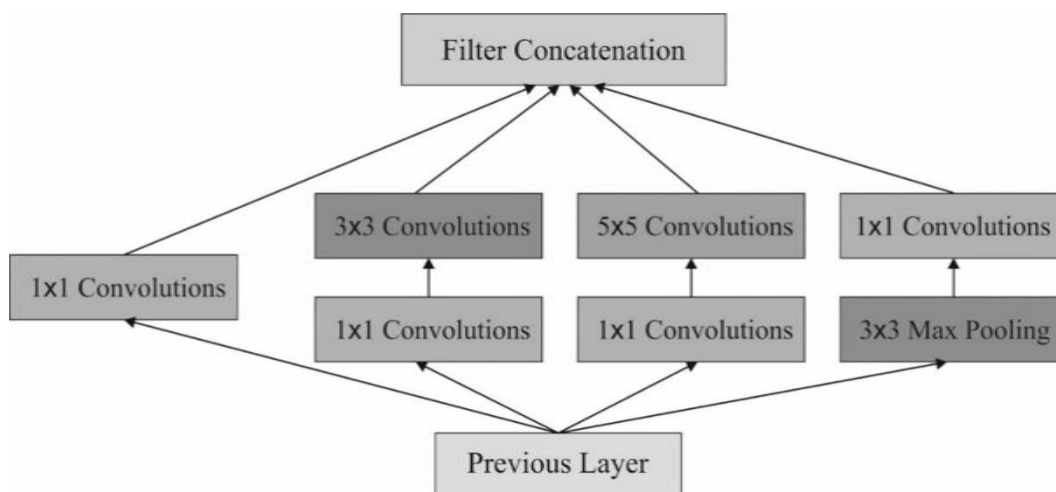


Fig. 5. Structure of Inception network

The GoogLeNet system is a CNN introduced by Google in the year of 2014. It has developed the Inception model with limited number of network parameters; however, it enhances the depth of the network. Therefore, it is extensively employed in image classification task. The main objective of GoogLeNet network is an Inception network structure, called Inception network [20]. Numerous versions of GoogLeNet are available such as Inception v1, Inception v2, Inception v3, Inception v4, and Inception-ResNet. Initially, the inception component is composed of 3 various sizes of convolution and maximum pooling.

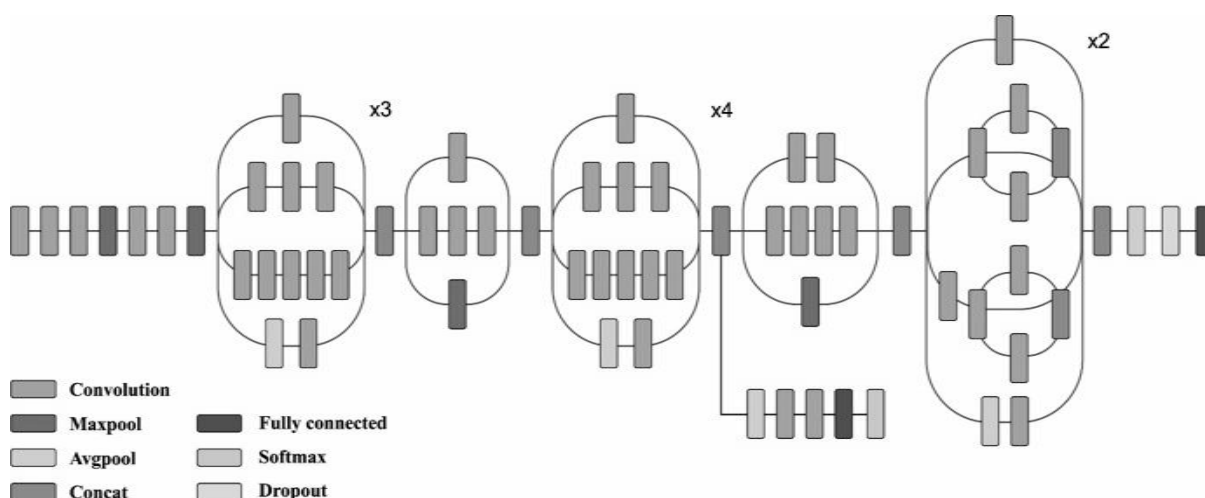


Fig. 6 Inception v3 Network structure

For a network output of former layer, the channel is collected next to convolution mechanism, and the nonlinear combination is performed. Likewise, the representation of a system and flexibility to distinct scales are enhanced and over-fitting could be eliminated. Fig.5 depicts the overall structure of Inception. At the same time, Inception v3 is defined as a network structure deployed by Keras. The default image has an input size of 299*299 with 3 channels. The Inception v3 network structure applied in this study is depicted in Fig. 4.

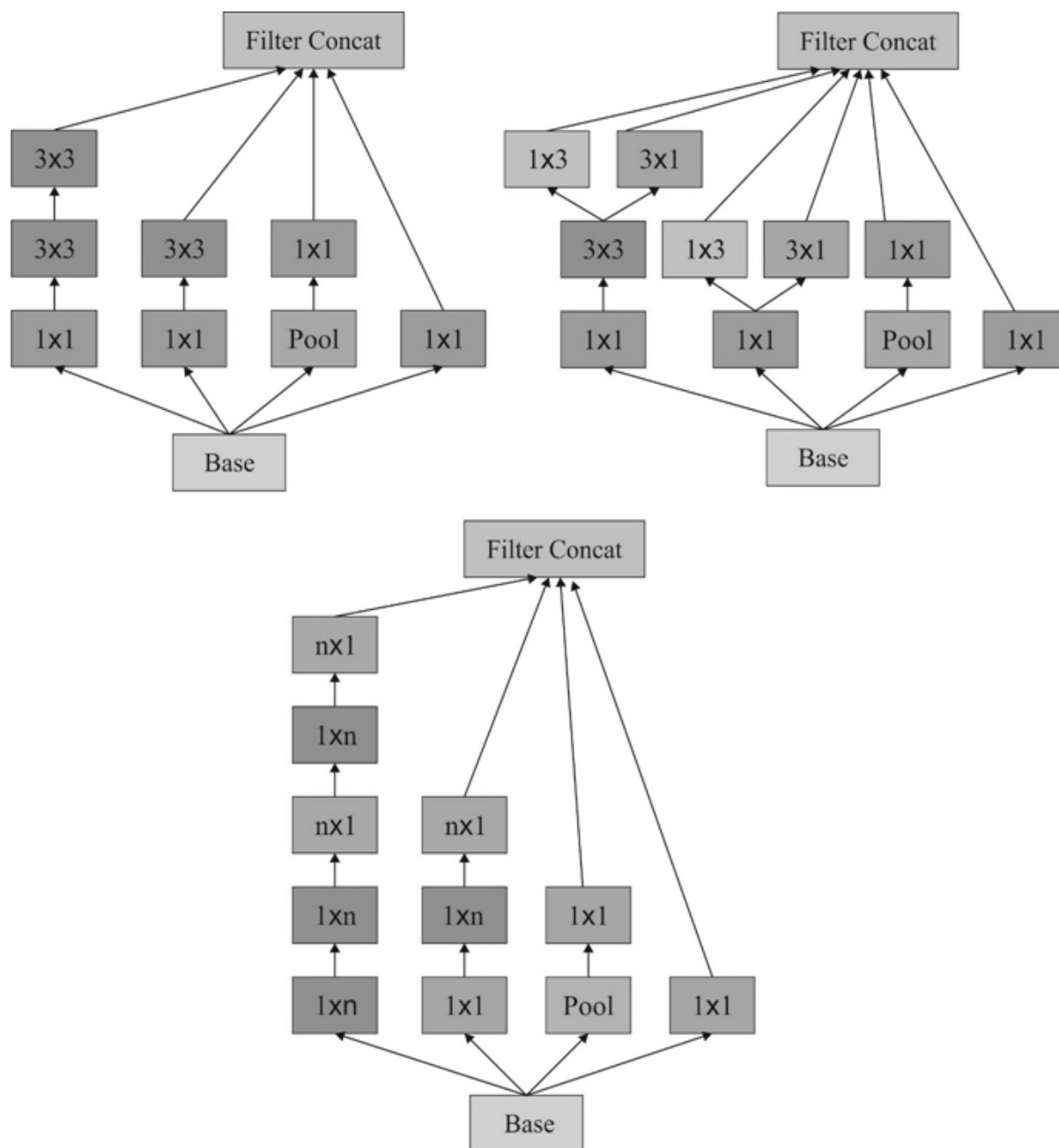


Fig. 7 Different sizes of Inception

On comparing with existing Inception models, Inception v3 architecture applies a convolution kernel splitting scheme for dividing massive integrals as tiny convolutions. For instance, a 3*3 convolution is divided as 3*1 and 1*3 convolutions. Under the application of splitting scheme, the parameter count could be limited; thus, the network training speed should be stimulated whereas spatial features are obtained significantly. Concurrently, Inception v3 optimizes the Inception network module by 3 various size area grids, as illustrated in Fig. 7.

D. Image Classification

At last, the extracted feature subsets are fed as input to the Gaussian Naïve Bayes and Logistic Regression models to perform the classification process.

1) GNB Model:

A Naive Bayes (NB) classification model measures the viability of the applied samples which belongs to a specific class [21]. Some of the instance X is defined by the corresponding feature vector (x_1, \dots, x_n) as well as class target y , conditional probability $P(y|X)$ is depicted as a combination of simple probabilities under the application of Naive independence assumption based on the Bayes' theorem:

$$P(y|X) = \frac{P(y)P(X|y)}{P(X)} = \frac{P(y) \prod_{i=1}^n P(x_i|y)}{P(X)}. \quad (9)$$

In this model, the target y is composed of 2 values in which $y = 1$ shows presence of BT as well as $y = 0$ implies absence of BT. Next, X for single residue is defined as a feature vector with identical size which defines the features under the application of high-frequency modes produced by GNM. When 3 high-frequency modes are considered as u_1, u_2 , and u_3 , where the vector $X(u_{1i}, u_{2i}, u_{3i})$ for residue i is present in a protein sequence. Additionally, while the window size is 3 interms of residue, X is assumed as $(u_{1i-1}, u_{1i}, u_{1i+1}, u_{2i-1}, u_{2i}, u_{2i+1}, u_{3i-1}, u_{3i}, u_{3i+1})$.

As $P(X)$ is a constant for given function where the following rule has been applied for classifying the instance of unknown class:

$$\hat{y} = \arg \max_y P(y) \prod_{i=1}^n P(x_i|y), \quad (10)$$

where "arg" refers a measure of y ; which means that if $P(y = 1) \prod_i P(x_i|y = 1)$ is greater than $P(y = 0) \prod_i P(x_i|y = 0)$, $\hat{y} = 1$; else, $\hat{y} = 0$. Furthermore, if the likelihood of features ($P(x_i|y)$) are considered as a Gaussian, an NB classification model named as GNB. Because of the simplicity and robust processing when compared with alternate sophisticated models, GNB is employed extensively for prediction issues involved in bioinformatics. The central premises of GNB are to train the presented methods by using high-frequency modes for the purpose of identifying BT.

2) Logistic Regression Classifier:

LR is defined as a commonly employed classifier, which is used to predict a binary related parameter. The dependent variable ranges from 0 or 1 values. Hence, the conditional probability for dependent attribute is provided in the following:

$$P\left(Y = \frac{1}{X}\right) = \pi(X) = \frac{e^{\beta'X}}{1 + e^{\beta'X}}, \quad (11)$$

where $\beta'X = \beta_0 + \beta_1 X_1 + \dots + \beta_k X_k$, and k implies count of autonomous variables. This expression is represented as $\pi(X)$ an S -Shaped function of independent parameters. Therefore, the probability distribution of dependent parameters is expressed as:

$$P(Y_i = y_i) = \begin{cases} \pi_i^{y_i} (1 - \pi_i)^{1-y_i} & y_i = 0 \text{ or } 1 \\ 0, & \text{otherwise.} \end{cases} \quad (12)$$

The likelihood function is defined as a combination of above-mentioned probabilities and logarithm of possibility function is demonstrated as follows:

$$\log_e L(\beta) = \sum_{i=1}^n Y_i (\beta'X_i) - \sum_{i=1}^n \log_e (1e + \exp(\beta'X_i)). \quad (13)$$

The variables of LR are evaluated through maximizing logarithmic probability function. Additionally, nonlinear optimization models are employed in maximizing logarithmic likelihood function. Moreover, an issue in LR is deciding autonomous variables [22]. Consequently, step-wise, backward and forward selection methodologies were preferred in this study.

E. Performance Validation

In this section, the simulation result analysis of the presented model is discussed. The simulation takes place on GeForce 1050Ti 4GB, 16GB RAM, 250GB SSD, and 1TB HDD. The simulation tool used is Python - 3.6.5 with different python packages namely tensorflow(GPU-CUDA Enabled), keras, numpy, pickle, matplotlib, sklearn, pillow, and OpenCV-python. The dataset involved, measures, and the results are discussed in the subsequent sections.

1) Dataset used:

In order to test the classifier results analysis, a benchmark MRI brain image dataset is utilized [23] that comprises an entirety of 147 tumor images. A set of 34 and 113 images comes under benign and malignant classes respectively. The image size varies between 630*630 and 192*192 pixels. Few of the sample benign and malignant class images are shown in Fig. 8.

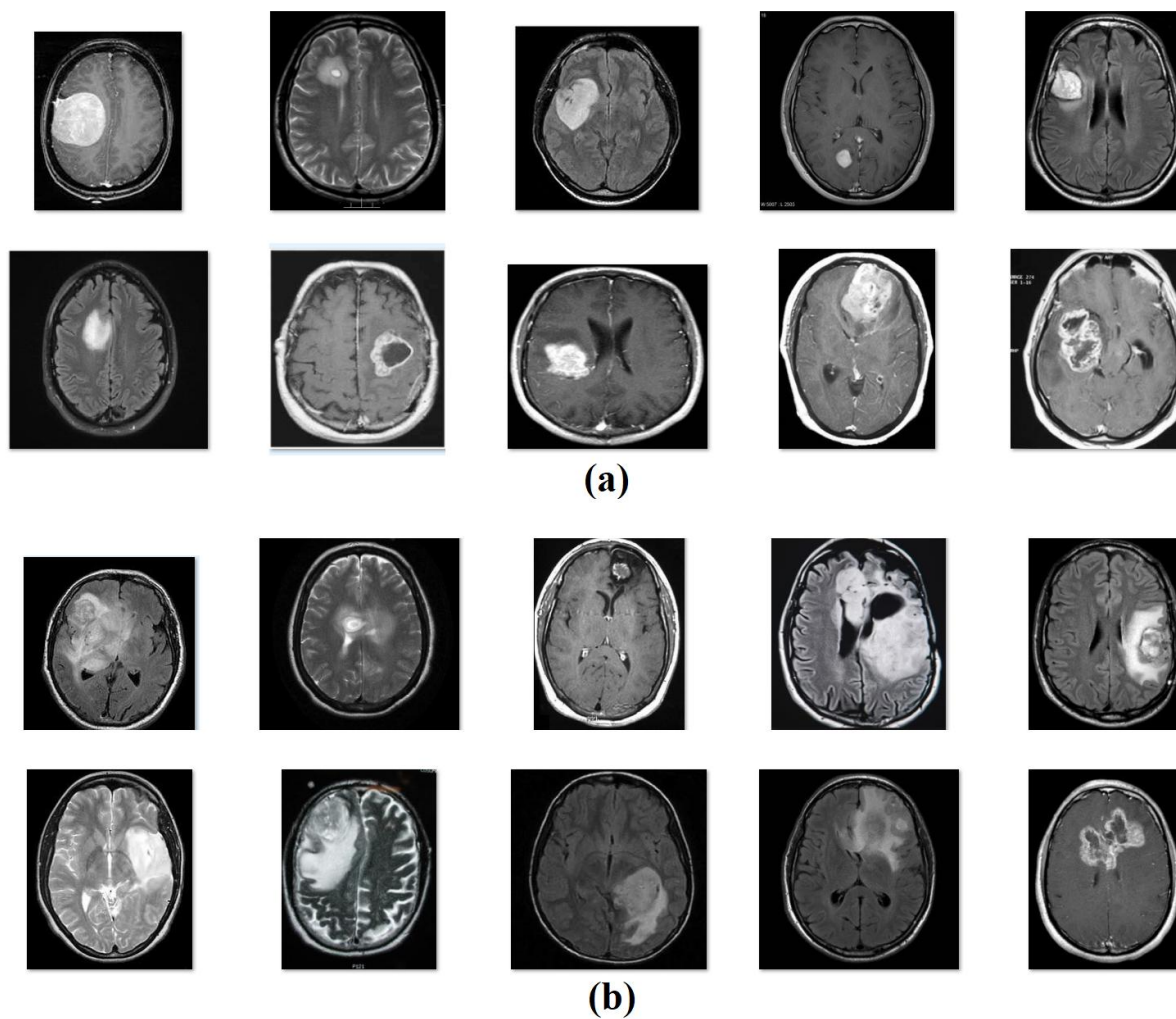


Fig. 8. Sample Images a) Benign b) Malignant

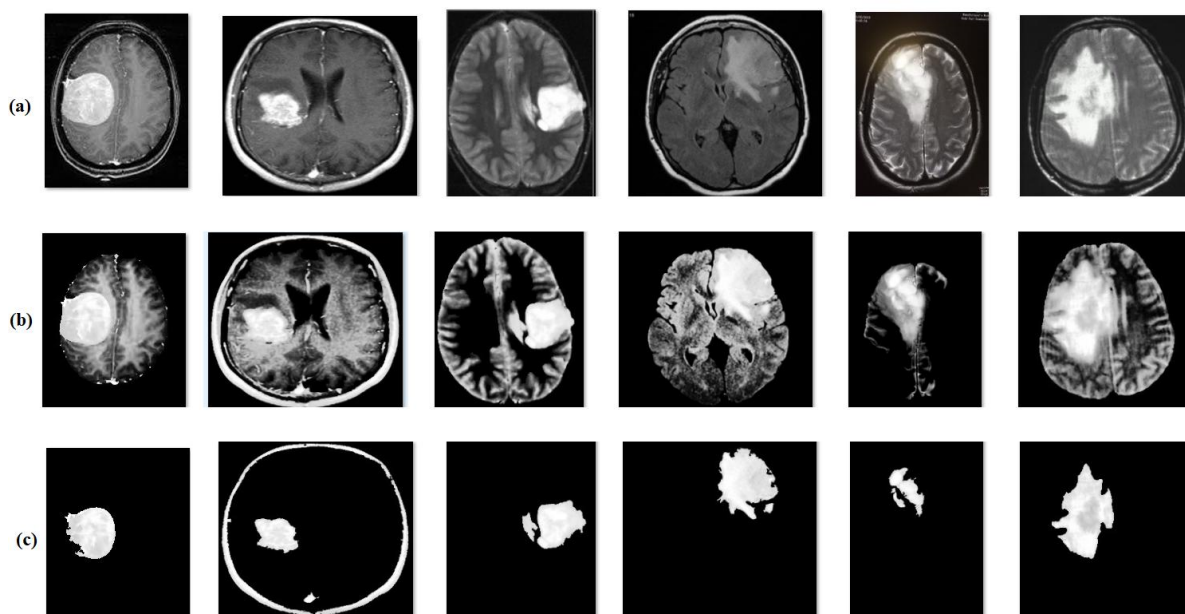
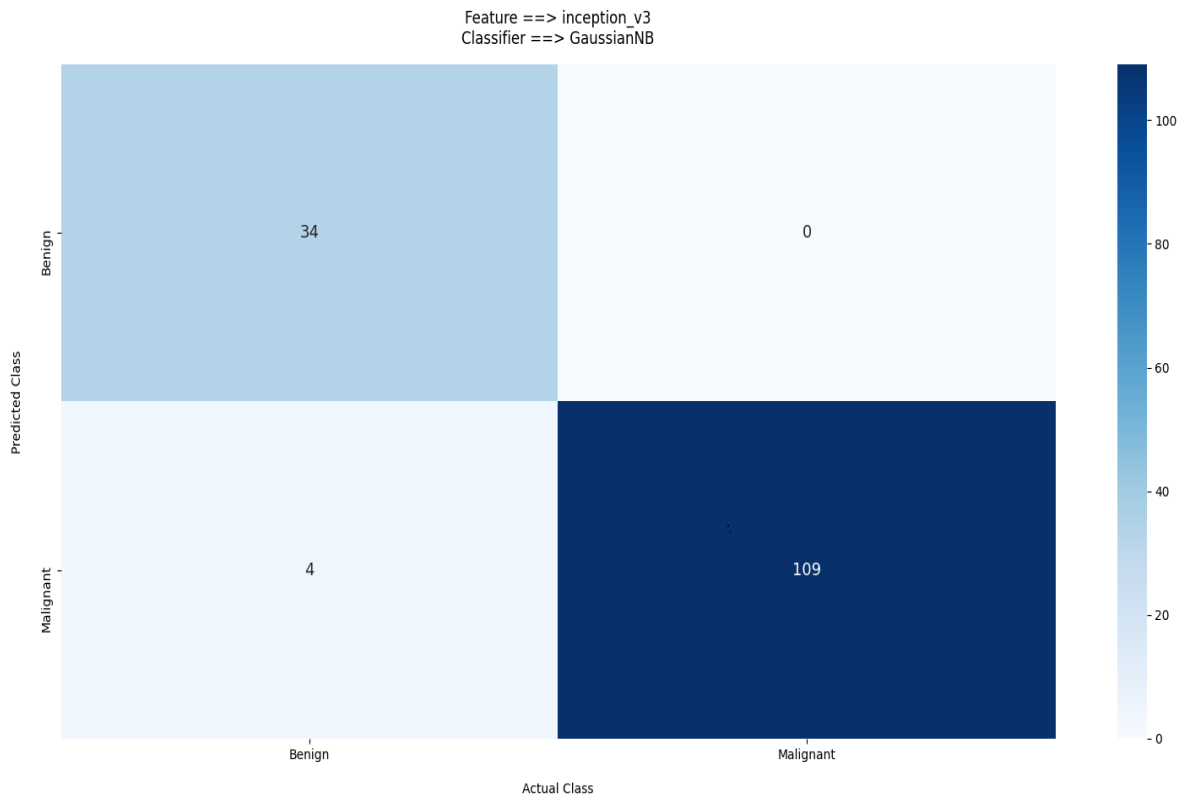
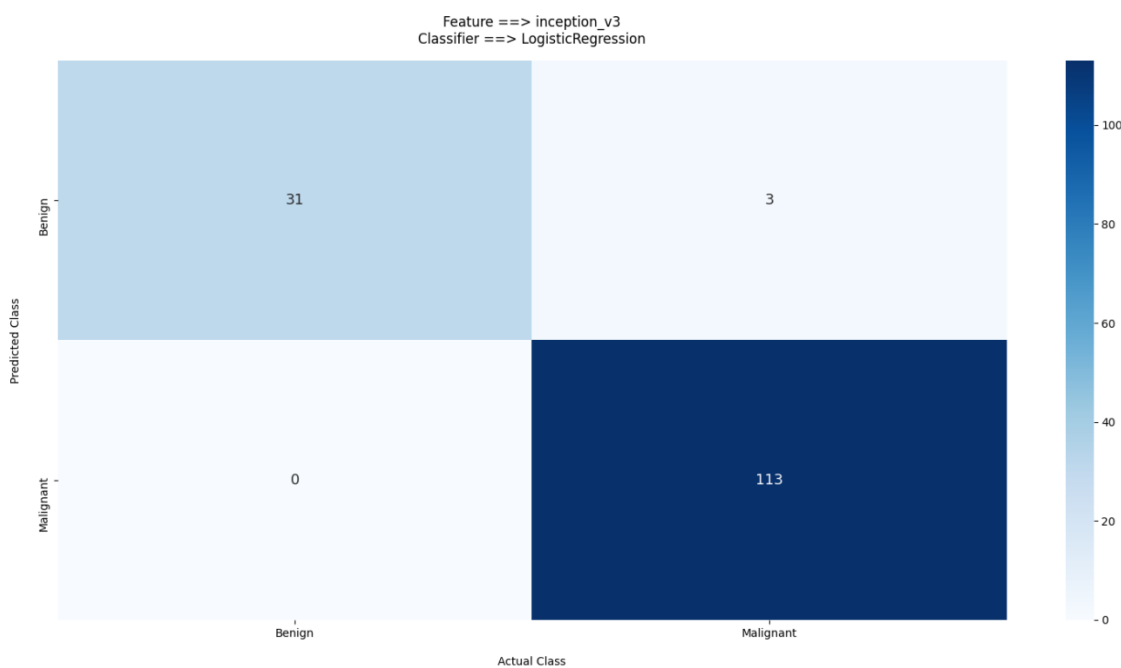


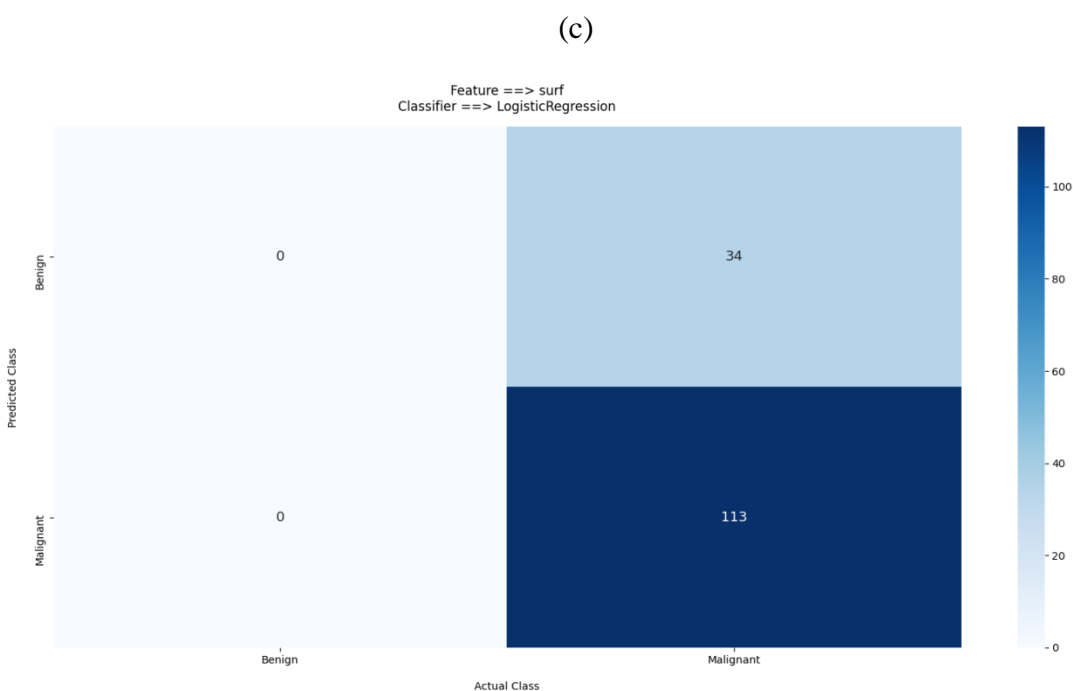
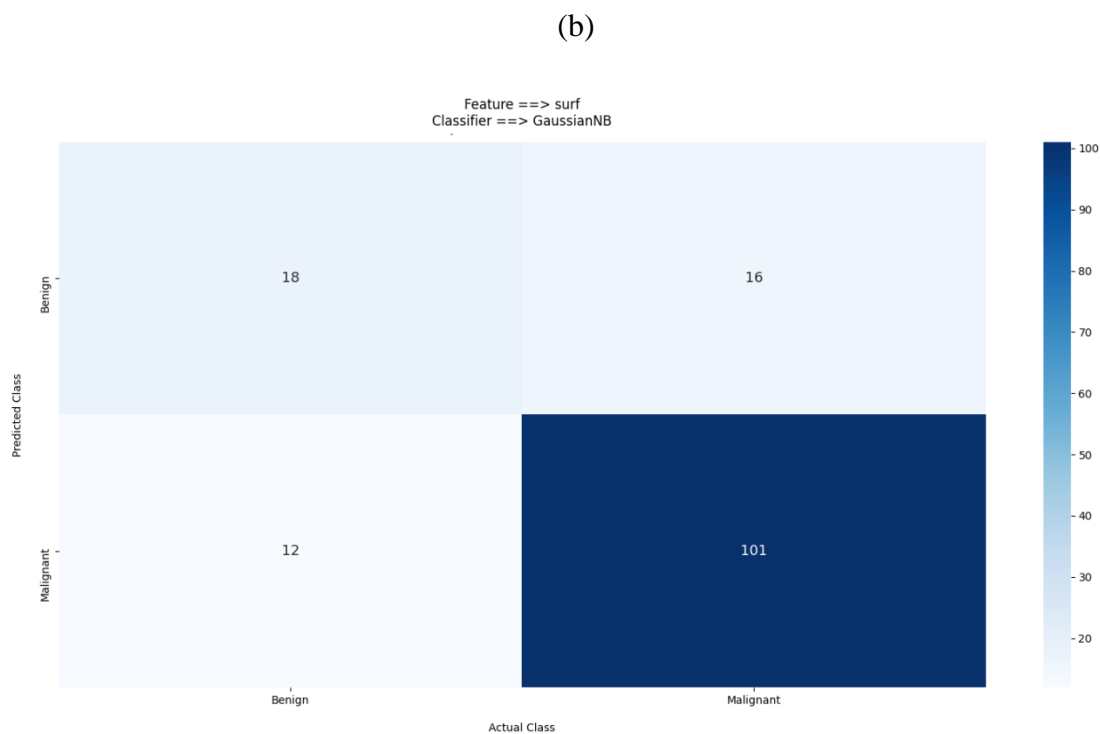
Fig.9. a) Original Images b) Preprocessed Outcome c) Segmented Outcome

A visualization of the results attained by the presented model is revealed in Fig. 9. The input original image is depicted in Fig. 9a, the resultant preprocessed and segmented images are displayed in Figs. 9b and 9c respectively. The figures shown that the presented model effectively preprocesses and identifies the tumor regions properly.



(a)





(d)

Fig. 10. Confusion Matrix a) DLIM-GNB b) DLIM-LR c) SURF- GNB d) SURF-LR

The confusion matrices produced by the different sets of proposed models are shown in Fig. 10. Fig. 10d exhibits that the SURF-LR model has effectively classified no images as benign and 113 images as malignant. Similarly, Fig. 10c showcased that the SURF-GNB model has proficiently classified a total of 18 images as benign and 101 images as malignant. Followed

by, Fig. 10a depicted the near optimal results of the DLIM-GNB model by classifying a total of 34 images as benign and 109 images as malignant. At last, Fig. 10b demonstrated that the DLIM-LR model has resulted to the classification of 31 images as benign and 113 images as malignant.

Table 1 and Fig. 11 summarize the classifier results analysis of the four proposed models interms of distinct evaluation parameters. On looking into the table, it is observed that the SURF-LR model has led to a least specificity of 76.87%, precision value of 87.54%, f-score of 54.23% and sensitivity of 74.82%. In addition, the SURF-GNB model has surpassed the SURF-LR model with the certainly higher sensitivity of 60%, specificity of 86.32%, accuracy of 80.95%, precision of 52.94%, and accuracy of 53.25%. Though the DLIM-GNB model has exhibited satisfactory classification outcome with a high sensitivity of 89.47%, specificity of 100%, accuracy of 97.28%, precision of 100%, and F-score of 94.44%. But the DLIM-LR model has shown proficient performance with the maximum sensitivity of 100%, specificity of 97.41%, accuracy of 97.96%, precision of 91.18%, and F-score of 95.38%.

Methods	Sensitivity(%)	Specificity(%)	Accuarcy(%)	Precision(%)	F-score(%)
DLIM-LR	100	97.41	97.96	91.18	95.38
DLIM-GNB	89.47	100	97.28	100	94.44
SURF-GNB	60.00	86.32	80.95	52.94	56.25
SURF-LR	74.82	76.87	76.87	87.54	54.23

Table 1 Result Analysis of Proposed Methods interms of distinct measures

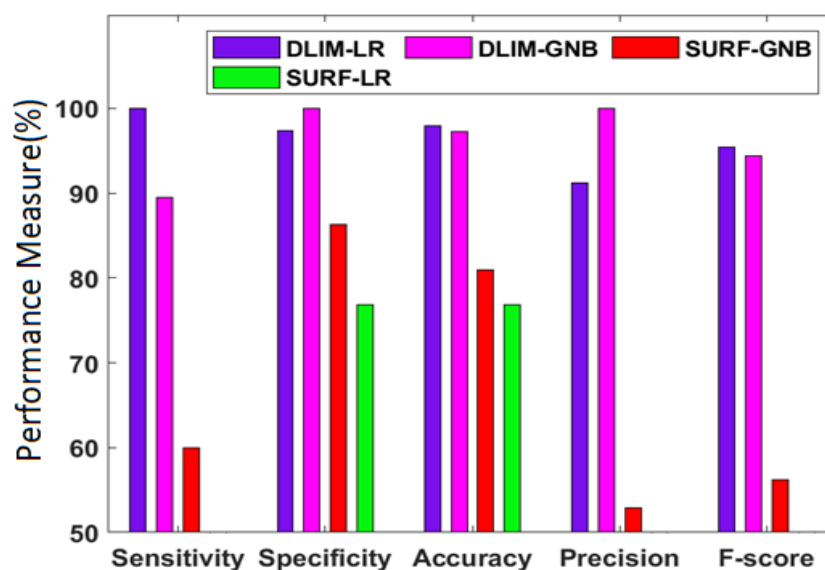


Fig. 11. Result analysis of DLIM-LR model with different model

Methods	Sensitivity(%)	Specificity(%)	Accuracy(%)	Precision (%)	F-score (%)
Proposed method					
DLIM-LR	100	97.41	97.96	91.18	95.38
Existing methods					
CNN-VGG16	81.25	88.46	89.66	84.48	85.25
ResNet-50	89.74	96.40	92.54	-	93.33
CART	88.00	80.00	84.00	-	-
Random Forest	90.00	80.00	88.00	-	-
k-NN	80.00	80.00	80.00	-	-
Linear SVM	91.20	80.00	88.00	-	-
ANFIS	96.20	95.10	96.40	-	-
CNN-CA	91.20	93.40	93.30	-	-
CNN	94.20	94.40	94.60	-	-
DCNN-CA	92.60	93.00	93.30	-	-
MABA	94.30	95.10	95.90	-	-

Table 2 Result Analysis of Existing with Proposed Methods interns of different measures

Table 2 and Figs. 11-12 implies the comparative results analysis of the DLIM-LR method with previous approaches [24-27] by means of various metrics. Fig. 10 examines the classifier results analysis of the DLIM-LR approach with respect to sensitivity, specificity, and accuracy. The experimental outcomes implied that the kNN scheme accomplished inferior performance by reaching minimum and closer sensitivity, specificity, and accuracy of 80%. Additionally, the CNN-VGG16 framework has attained moderate sensitivity of 81.25%, specificity of 88.46%, and accuracy of 89.66%. In line with this, the CART technique has resulted in considerable sensitivity of 88%, specificity of 80%, and accuracy of 84%. Simultaneously, the ResNet-50 scheme has attempted to gain acceptable sensitivity of 89.74%, specificity of 96.4%, and accuracy of 92.54%. At the same time, the RF framework has obtained better results with a sensitivity of 90%, specificity of 80%, and accuracy of 88%.

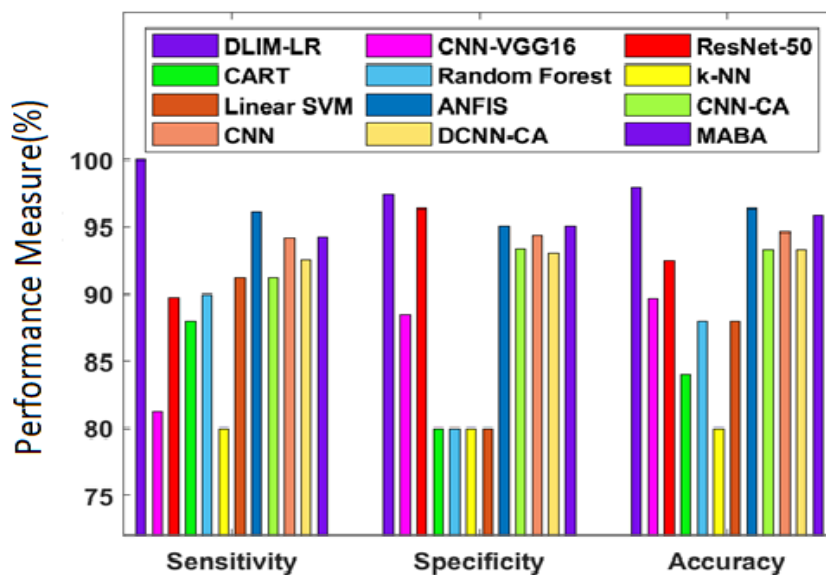


Fig. 12. Comparative analysis of DLIM-LR model

Followed by, the linear SVM has represented convincing outcomes with a sensitivity of 91.2%, specificity of 80%, and accuracy of 88%. Similarly, the CNN-CA method has depicted moderate results with sensitivity of 91.20%, specificity of 93.4%, and accuracy of 93.3%. Meantime, the DCNN-CA approach has accomplished slightly better results with the sensitivity of 92.6%, specificity of 93%, and accuracy of 93.3%. Meantime, the CNN framework has represented maximum outcomes than existing methodologies with the sensitivity of 94.2%, specificity of 94.4%, and accuracy of 94.6%. Moreover, the MABA scheme has surpassed the moderate result with the sensitivity of 94.3%, specificity of 95.1%, and accuracy of 95.9%. Although the ANFIS scheme has implied competing results with the sensitivity of 96.2%, specificity of 95.1%, and accuracy of 96.4%, it is insignificant to perform well than the presented DLIM-LR approach which has gained higher sensitivity of 100%, specificity of 97.41%, and accuracy of 97.96%.

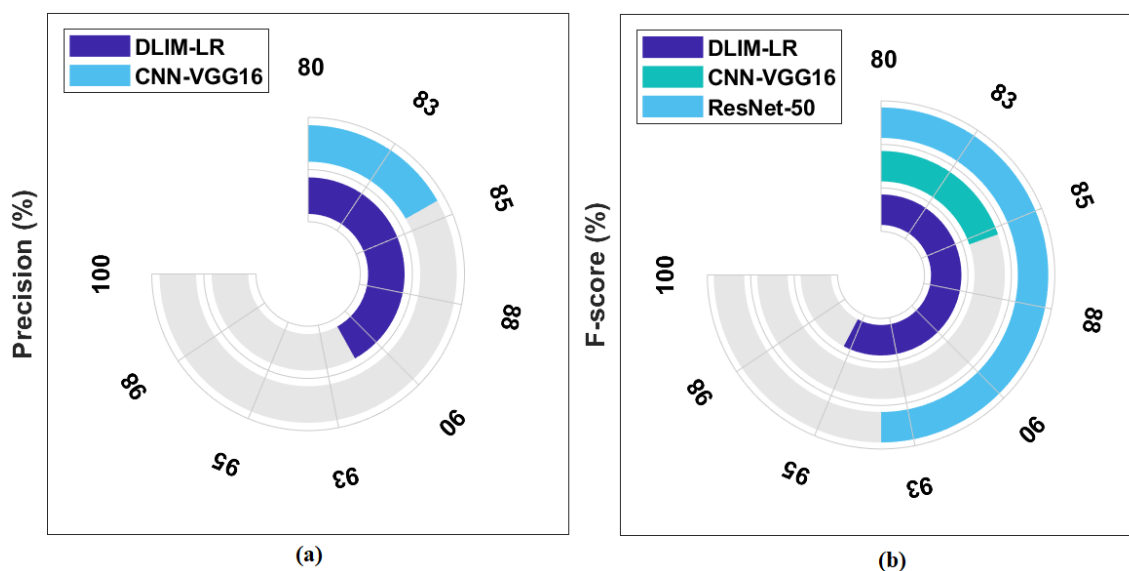


Fig. 13. Comparative analysis of DLIM-LR model interms of precision and F-score

Fig. 13 investigates the classifier result analysis of the DLIM-LR model interms of precision and F-score. The performance results have showcased that the CNN-VGG16 method accomplished inferior results by gaining inferior precision of 84.48% and F-score of 85.25%. Furthermore, the ResNet-50 mechanism has achieved better F-score of 93.33%. Thus, the proposed DLIM-LR framework has achieved maximum precision of 91.18% and F-score of 95.38%.

F. Conclusion

This study has introduced a new BT diagnosis model using SURF and Inception network. Primarily, the input image is pre-processed to strip the skull, remove the noise, and increase the contrast level. Then, FCM based segmentation technique is employed to identify the diseased portions in the image. Afterward, the SURF and Inception v3 models are applied to extract a useful set of feature vectors. At last, GNB and LR models are utilized of classification processes. To validate the results analysis of the presented technique, a series of experiments take place on the benchmark dataset. The simulation outcome verified the supremacy of the proposed DLIM-LR model on the diagnosis of BT with the maximum sensitivity of 100%, specificity of 97.41%, and accuracy of 97.96%. In future, the diagnostic outcome of the proposed model can be improved using dissimilar feature extractor and classifier technique.

References

- [1] Development of deep learning algorithm using convolutional neural network for medical imaging. *Int J EngAdvTechnol* 2020;9(3):139–42.
- [2] Talo M, Baloglu UB, Yildirim Ö, RajendraAcharya U. Application of deep transfer learning for automated brain abnormality classification using MR images. *CognSyst Res* 2019;54:176–88.
- [3] Alqazzaz S, Sun X, Yang X, Nokes L. Automated brain tumor segmentation on multi-modal MR image using SegNet. *Comput Vis Media* 2019;5(2):209–19.
- [4] Sugimori H, Kawakami M. Automatic detection of a standard line for brain magnetic resonance imaging using deep learning. *ApplSci (Basel)* 2019;9(18):3849.
- [5] Ismail M, et al. A fast stochastic framework for automatic MR brain images segmentation. *PLoS One* 2017;12(11):e0187391.
- [6] Siva Raja PM, Rani AV. Brain tumor classification using a hybrid deep autoencoder with Bayesian fuzzy clusteringbased segmentation approach. *Biocybern Biomed Eng* 2020;40(1):440–53.
- [7] Gumaste PP, Bairagi DVK. A hybrid method for brain tumor detection using advanced textural feature extraction. *Biomed Pharmacol J* 2020;13(1).
- [8] Gumaei A, Hassan MM, Hassan MR, Alelaiwi A, Fortino G. A hybrid feature extraction method with regularized extreme learning machine for brain tumor classification. *IEEE Access* 2019;7:36266–73.
- [9] Sharif M, Amin J, Raza M, Yasmin M, Satapathy SC. An integrated design of particle swarm optimization (PSO) with fusion of features for detection of brain tumor. *Pattern RecognitLett* 2020;129:150–7.

- [10] Hong KS, Khan MJ, Hong MJ. Feature extraction and classification methods for hybrid fNIRS-EEG braincomputer interfaces. *Front Hum Neurosci* 2018;12. Frontiers Media S.A..
- [11] Bernal J, et al. Deep convolutional neural networks for brain image analysis on magnetic resonance imaging: a review. *ArtifIntell Med* 2019;95:64–81.
- [12] Seetha J, Raja SS. Brain tumor classification using convolutional neural networks. *Biomed Pharmacol J* 2018;11(3):1457–61.
- [13] Wang K, Savva M, Chang AX, Ritchie D. Deep convolutional priors for indoor scene synthesis. *ACM Trans Graph* 2018;37(4).
- [14] Zhang Y, Xiang T, Hospedales TM, Lu H. Deep mutual learning. *Proceedings of the IEEE computer society conference on computer vision and pattern recognition*; 2018;4320–8.
- [15] Kushibar K, et al. Automated sub-cortical brain structure segmentation combining spatial and deep convolutional features. *Med Image Anal* 2018;48:177–86.
- [16] Khoshaman A, Vinci W, Denis B, Andriyash E, Sadeghi H, Amin MH. Quantum variational autoencoder. *Quantum SciTechnol* 2018;4(1):014001.
- [17] Li, M.Q., Xu, L.P., Xu, N., Huang, T. and Yan, B., 2018. SAR image segmentation based on improved grey wolf optimization algorithm and fuzzy c-means. *Mathematical Problems in Engineering*, 2018.
- [18] Fu, J., Jing, X., Sun, S., Lu, Y. and Wang, Y., 2012, May. C-surf: Colored speeded up robust features. In *International Conference on Trustworthy Computing and Services* (pp. 203-210). Springer, Berlin, Heidelberg.
- [19] Garikapati, P., Balamurugan, K., Latchoumi, T. P., & Malkapuram, R. (2020). A Cluster-Profile Comparative Study on Machining AlSi 7/63% of SiC Hybrid Composite Using Agglomerative Hierarchical Clustering and K-Means. *Silicon*, 1-12.
- [20] Mahdianpari, M., Salehi, B., Rezaee, M., Mohammadimanesh, F. and Zhang, Y., 2018. Very deep convolutional neural networks for complex land cover mapping using multispectral remote sensing imagery. *Remote Sensing*, 10(7), p.1119.
- [21] Ezhilarasi, T. P., Kumar, N. S., Latchoumi, T. P., & Balayesu, N. (2021). A Secure Data Sharing Using IDSS CP-ABE in Cloud Storage. In *Advances in Industrial Automation and Smart Manufacturing* (pp. 1073-1085). Springer, Singapore.
- [22] Dong, N., Zhao, L., Wu, C.H. and Chang, J.F., 2020. Inception v3 based cervical cell classification combined with artificially extracted features. *Applied Soft Computing*, p.106311.
- [23] Zhang, H., Jiang, T. and Shan, G., 2016. Identification of hot spots in protein structures using Gaussian network model and Gaussian Naive Bayes. *BioMed research international*, 2016.
- [24] Tunç, T., 2012. A new hybrid method logistic regression and feedforward neural network for lung cancer data. *Mathematical problems in engineering*, 2012.
- [25] Sekaran, K., Rajakumar, R., Dinesh, K., Rajkumar, Y., Latchoumi, T. P., Kadry, S., & Lim, S. (2020). An energy-efficient cluster head selection in wireless sensor network using grey wolf optimization algorithm. *TELKOMNIKA*, 18(6), 2822-2833.
- [26] <https://www.kaggle.com/navoneel/brain-mri-images-for-brain-tumor-detection>

- [27] Latchoumi, T. P., Vasanth, A. V., Bhavya, B., Viswanadapalli, A., & Jayanthiladevi, A. (2020, July). QoS parameters for Comparison and Performance Evaluation of Reactive protocols. In 2020 International Conference on Computational Intelligence for Smart Power System and Sustainable Energy (CISPSSE) (pp. 1-4). IEEE.
- [28] Toğaçar, M., Ergen, B. and Cömert, Z., 2020. BrainMRNet: Brain tumor detection using magnetic resonance images with a novel convolutional neural network model. *Medical Hypotheses*, 134, p.109531.
- [29] Çınar, A. and Yıldırım, M., 2020. Detection of tumors on brain MRI images using the hybrid convolutional neural network architecture. *Medical Hypotheses*, p.109684.
- [30] Gupta, T., Gandhi, T.K., Gupta, R.K. and Panigrahi, B.K., 2017. Classification of patients with tumor using MR FLAIR images. *Pattern Recognition Letters*.
- [31] Selvapandian, A. and Manivannan, K., 2018. Fusion based glioma brain tumor detection and segmentation using ANFIS classification. *Computer methods and programs in biomedicine*, 166, pp.33
- [32] ArunaKirithika.R, Sathiya.S et. al.,2020. Brain Tumor and Intracranial Haemorrhage Feature Extraction and Classification using Conventional and Deep Learning methods. *European Journal of Molecular and Clinical Medicine*.
- [33] Arunkarthikeyan, K., & Balamurugan, K. (2021). Experimental Studies on Deep Cryo Treated Plus Tempered Tungsten Carbide Inserts in Turning Operation. In *Advances in Industrial Automation and Smart Manufacturing* (pp. 313-323). Springer, Singapore.
- [34] Sathiya.S, Balasubramanian.M, Palanivel.S., 2013, Detection and Recognition of Characters in Place Name Board for Driving. *International Journal of Computer Applications (0975 8887) Volume 80 - No. 7*
- [35] S. Sathiya et al. 2014, Pattern Recognition Based Detection Recognition of Traffic Sign Using SVM, *International Journal of Engineering and Technology (IJET) Vol 6 No 2 Apr-May 2014*
- [36] Sneha, P., Balamurugan, K., & Kalusuraman, G. (2020, December). Effects of Fused Deposition Model parameters on PLA-Bz composite filament. In *IOP Conference Series: Materials Science and Engineering* (Vol. 988, No. 1, p. 012028). IOP Publishing.
- [37] Yarlagaddaa, J., Malkapuram, R., & Balamurugan, K. (2021). Machining Studies on Various Ply Orientations of Glass Fiber Composite. In *Advances in Industrial Automation and Smart Manufacturing* (pp. 753-769). Springer, Singapore.